Eur. Phys. J. D **33**, 405–411 (2005)
DOI: 10.1140/epjd/e2005-00075-y

THE EUROPEAN PHYSICAL JOURNAL D

Electronic properties of mixed lithium-oxygen clusters

J. Viallon, M.A. Lebeault[a], F. Lépine, J. Chevaleyre, C. Jonin, A.R. Allouche, and M. Aubert-Frécon

Laboratoire de Spectrométrie Ionique et Moléculaire, CNRS UMR N° 5579 et Université Lyon I,
43 boulevard du 11 novembre 1918, 69622 Villeurbanne Cedex, France

Received 6 December 2004
Published online 24 May 2005 –

Abstract. Herein electronic structure as a function of cluster size has been probed through ionization potentials measurements in order to derive general trends in the evolution of the structure and stability of lithium oxide clusters Li_nO_m. The structural evolution was investigated by varying progressively the oxygen rate in order to observe transitions from the metallic Li_n to the ionic structure $(Li_2O)_n$. We have demonstrated that this structural transition splits into three specific ranges. This result, in contrast with the general behavior observed with other electronegative elements combined with alkaline or alkaline-earth metal clusters, but similar to what is known about Ba_nO_m and Cs_nO_m, constitutes a signature of a specific role played by the oxygen atoms when included inside a metallic cluster.

PACS. 36.40.Mr Spectroscopy and geometrical structure of clusters – 33.15.Ry Ionization potentials, electron affinities, molecular core binding energy

1 Introduction

Electronegative elements (X), embedded in metallic clusters (M_nX_m) give rise to various changes in electronic properties depending on the metal concentration. On one hand stoechiometric clusters $(MX)_n$ present a structure close to the corresponding bulk, which is often an insulating crystal. Recent studies devoted to hydrides $(LiH)_m$ [1] and oxides $(MgO)_n$ [2,3], $(CaO)_n$ [4], $(BaO)_n$ [5] and $(ZrO_2)_n$ [6] clusters show that the equilibrium geometry of these species is of cubic symmetry and that the binding between metal and electronegative elements is ionic. On the other hand, pure metallic clusters M_n, and in particular alkaline clusters, are well known to have a metallic behavior, being characterized among others by a valence electrons delocalization in all the cluster volume. Among both, the structure of mixed M_nX_m clusters remains puzzling.

Two studies devoted to Li_nH_m [7] and Na_nF_m [8] ($n > m$) clusters show clear evidences of a segregation between an ionic part $(MX)_m$ and the excess metallic one $M_{p=n-m}$. However the case of mixed metal-oxygen clusters appears more surprising if one refers to what is known about Ba_nO_m clusters. Indeed, it has first been observed by TP Martin [4] that adding a small number of oxygen atoms (< 5) remains the icosahedral close packing structure of pure Ba_n clusters. This has been confirmed in our previous study on small Ba_nO_m ($n = 2$ to 13, $m = 0$ to n) clusters by ionization potentials measurements completed by ab-initio calculations [5,9]. This last work shows that the transition between pure and stoechiometric clusters regarding to a structural evolution is due to the forced reorganization of the cluster when the ratio of oxygen atoms in the cluster reaches 60%. In particular it has been demonstrated that the oxygen atoms tend to be surrounded by an important number of barium atoms by means of iono-covalent bond. This remark is also coherent with the experimental results derived from laser excitation of Cs_nO_m clusters [10]. The question of the more general character of this particular role of oxygen among other electronegative elements arises from such observation. It has conducted us to propose a study of mixed lithium-oxygen clusters where the oxygen rate is varying. Regarding to barium clusters, lithium clusters represent typical metallic ones. Indeed, Dugourd et al. have shown that Li_n clusters are described by the jellium model [11]. In particular, odd-even alternations as well as shell closing effects appear in their ionization potentials. Furthermore, this behavior still occurs for the metallic part Li_p of the $(Li_2O)Li_p$ clusters studied by Lievens et al. [12]. According to this last result, the possible particularity of oxygen among other electronegative elements is still relevant. In this paper we report on the measurements of ionization potentials of $(Li_2O)_mLi_p$ clusters with $1 < m < 15$ and $0 < p < 28$. These results are compared to calculations performed by Density Functional Theory approach using the Perdrew-Wang functional (1991).

2 Experimental set-up

Mixed lithium oxygen clusters are produced in a laser vaporization source and analyzed in a Wiley-Mc Laren

[a] e-mail: lebeault@lasim.univ-lyon1.fr

time-of-flight mass spectrometer (TOFMS) both described in details elsewhere [13]. To obtain lithium clusters, the laser vaporization is achieved by focusing a frequency tripled Nd^{3+}:YAG laser (355 nm, 12 ns, 20 mJ per pulse) or a frequency doubled Ti:sapphire laser (400 nm, 30 ns, 4 mJ per pulse) on a rotating, translating 6 mm-diameter isotopic lithium rod. A pulsed piezo molecular beam valve is used to deliver a short pulse of carrier gas that cools down the laser-induced plasma. A better cooling is obtained with a liquid nitrogen circulation surrounding the source. Helium carrier gas seeded with dioxygen has permitted to produce Li_nO_m clusters. Using two different concentrations of O_2: 500 ppm and 1%, we were able to produce a large distribution of Li_nO_m clusters, from the metal-rich Li_nO to the stoechiometric $(Li_2O)_m$. Two different laser systems have been employed for the threshold photoionization measurements. A lambda-physik dye laser pumped by an excimer laser provides photons from 3.0 to 5.8 eV. More recently, we made the acquisition of an optical parametric oscillator (OPO Surelite Continuum) pumped by the third harmonic of a seeded Nd^{3+}:YAG. This system is used to cover energy ranging from 3.65 to 4.77 eV; and from 2.7 to 3.0 eV by frequency doubling. The 3.0–3.65 eV gap is covered by use of the dye laser. The ionic clusters so formed enter the TOFMS where the ion signal is recorded by means of a micro-channel plate coupled with a digital oscilloscope (Lecroy 9300) interfaced to a laboratory PC. Full time of flight mass spectra are recorded at each ionization laser wavelength in order to derive photoionization curve for each cluster size.

3 Results

3.1 Experimental results

In order to obtain different oxygenation rates of lithium cluster oxygenated species we used two kinds of carrier gas: He 6.0 + 500 ppm of O_2 to produce low oxygenated clusters species Li_nO, Li_nO_2 and Li_nO_3; and He 6.0 + 1% of O_2 to produce species close to the stoechiometry $(Li_2O)_n$ and $Li(Li_2O)_n$. Notice that using light element like lithium which presents a non negligible amount of isotopes rapidly produces in mass spectra a peak for every mass value. As a consequence and in order to ensure a confident mass interpretation in our spectra we used the ^{7}Li isotopic compound. With such material the first mass overlap occurs for clusters with $Li_{16n}O_m = Li_{16(n-1)}O_{m+7}$ the first one concerned is $Li_{32}O$ which presents the same mass peak than $Li_{16}O_8$. Such mass overlap results in a mass attribution limitation in our mass spectra interpretation; it wouldn't be suitable to attribute mass peak above 240 u.m.a. This remark is only valid for series Li_nO_m with $m \geq 7$; as no overlap can occur the mass peak attribution is only limited by the TOFMS resolving power. Furthermore lithium is highly reactive with electronegative elements like hydrogen; as a consequence water adsorption that occurs on the lithium rod surface gives rise, during the laser vaporization, to hydrogenated compounds that increase considerably the number of indesirable peaks. To avoid this phenomenon, a preliminary vaporization session was necessary to clean the rod surface in order to produce water and hydrogen free clusters.

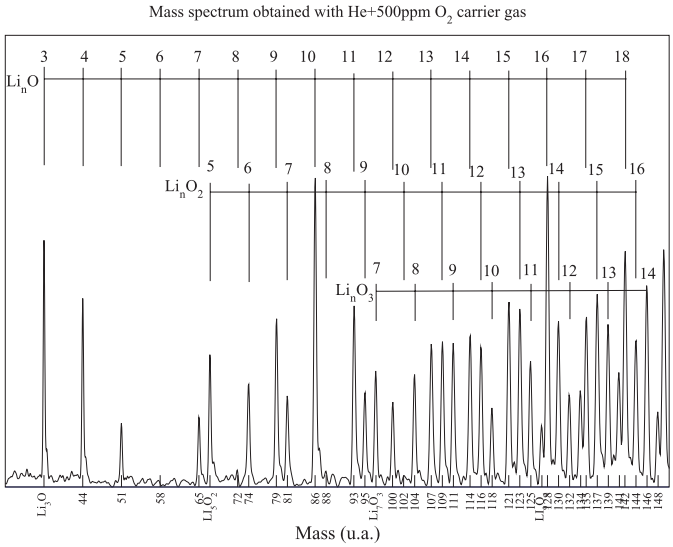

Fig. 1. Mass spectrum of lithium oxide clusters obtained with 500 ppm of O_2 in helium.

Clusters obtained under the condition of low oxygenation, i.e. with 500 ppm of O_2 in He carrier gas

A typical spectrum is shown in Figure 1. With such spectra we were able to investigate cluster sizes up to $Li_{30}O_m$ with $m = 1, 2, 3, 4, 5...$ with a decreasing signal intensity depending on the m increasing value. The goal is to observe a sufficiently large amount of Li_nO_m series in order to investigate all the oxygenated rate from 0 to 0.5 in the recorded Li_nO_m peaks. Under these conditions the low oxygenated series are well identified and especially the $Li_{n\leq 30}O$, $Li_{n\leq 28}O_2$ and $Li_{n\leq 26}O_3$ clusters families are the most intense. The nucleation process conditions involved here do not lead to the formation of the stoechiometric $(Li_2O)_m$ clusters. Indeed, the Li_4O_2 and Li_6O_3 clusters are absent in the spectrum (respectively mass 60 amu and 90 amu), while the used wavelength allows their observation as seen with the other carrier gas. To conclude, these spectra have been devoted to the ionization potential measurements of Li_nO, Li_nO_2 and Li_nO_3 clusters.

Clusters obtained under the condition of high oxygenation, i.e. with 1% of O_2 in He carrier gas

A typical spectrum is shown in Figure 2. Owing to the high oxygen rate such spectra exhibit a strong signal for the near stoechiometric and stoechiometric clusters: $(Li_2O)_m$ and $(Li_2O)_mLi$ up to $m = 16$. These spectra have conducted to the ionization potential measurements of those species.

Various empirical methods can be applied to determine ionization potentials (*IP*s) from photoionization efficiency

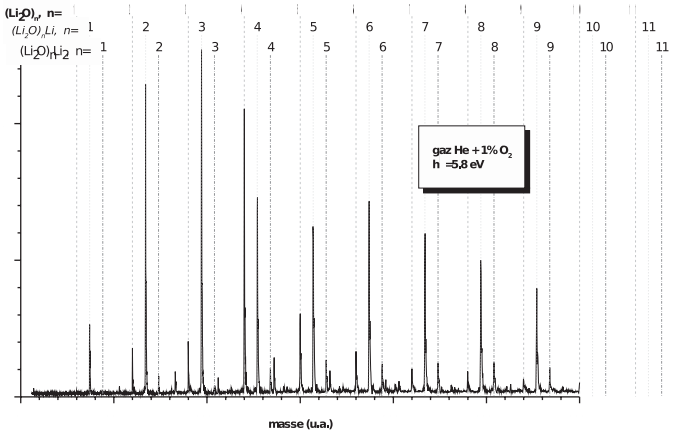

Fig. 2. Mass spectrum of Li_nO_m clusters obtained with 1% of O_2 in helium.

(PIE) curves [10,14–17]. We used the most straightforward procedure which is widely applied for clusters. In a PIE curve the intercept of the baseline and the first linear increase is used to determine the ionization potential. This method is called linearization procedure; it has been described in an earlier paper [18]. It has to be noticed that, in order to produce only the most stable isomers, we used a liquid nitrogen cooled cluster source. We have listed the ionization potential measurements in Table 1.

3.2 Calculation method

To reveal the origin of the some special stabilities discussed further, and to learn the structural trends in the lithium oxide neutral distribution, Li_nO_m structures with $n \leq 10$ and $m \leq 3$ are calculated. We have although determined the ionization potential of each species in order to compare them with the experimental data. $Li_{n=3...10}O$, $Li_{n=4...11}O_2$ and $Li_{n=6...9}O_3$ clusters systems are calculated employing density functional theory (DFT) and the ab-initio Hartree-Fock method as implemented in GAUSSIAN98 [19]. The DFT gradient corrected correlation functional (Perdrew and Wang) [20] and the gradient corrected exchange functional [21] are employed with the Gaussian98 program (BPW91). All three electrons for lithium atom and eight electrons for each oxygen atom are treated explicitly. The $631G$ basis set has been employed throughout these calculations to obtain the cluster geometry and energy of the most stable isomers. All geometry optimization are performed for the cluster ground electronic state and with full relaxation of all geometric coordinates. Clusters of these sizes may have many stable isomers corresponding to different local minima on the cluster potential hypersurface. For each cluster size, geometry optimization were performed starting from a number of initial geometrical configurations to maximize chances of finding the most stable isomer (the global minima on the cluster potential surface). This procedure allows to calculate the lowest energy level among isomers of each cluster size. Indeed, energies are roughly estimated from a

Table 1. Ionization potentials of Li_nO_m clusters. The uncertainty is ± 0.02 eV for $Li_nO_{1,2,3}$ and $(Li_2O)_mLi$ clusters and ± 0.03 eV for $(Li_2O)_m$ clusters.

Number of lithium atoms	n Li_nO	Li_nO_2	Li_nO_3	...	$(Li_2O)_mLi$ $n = 2m+1$	$(Li_2O)_m$ $n = 2m$
3	3.55				3.55	
4	4.16	4.96				4.96
5	4.05	2.64			2.64	
6	4.70	3.65	4.96			4.96
7	4.05	3.44	2.56		2.56	
8	4.25	3.95	3.45			4.82
9	3.87	3.48	3.44		2.61	
10	4.05	3.80	3.69			4.88
11	3.65	3.48	3.46		2.65	
12	4.00	3.80	3.49			4.93
13	3.69	3.67	3.41		2.68	
14	3.90	3.80	3.50			5.02
15	3.39	3.44	3.42		2.65	
16	3.46	3.83	3.50			5.02
17	3.44	3.52	3.42		2.72	
18	3.50	3.69	3.55			5.02
19	3.32	3.48	3.32		2.76	
20	3.42	3.56	3.44			
21	3.30	3.48	3.38		2.76	
22	3.42	3.52	3.41			
23	3.30	3.46	3.39		2.72	
24	3.46	3.48	3.42			
25	3.39	3.42	3.44		2.74	
26	3.44	3.48	3.44			
27	3.41	3.41	3.42		2.54	
28	3.39	3.44	3.42			
29	3.41	3.42	3.44			
30	3.41	3.41	3.42			
31		3.40	3.41		2.75	
32		3.41	3.33			
33		3.37	3.39			
34		3.37	3.34			
35			3.39			

pair-wise semi-empirical potential designed as the sum of a long-range type charge-charge interaction plus an exponential term simulating exchange and penetration effects. The expression of this potential is as follows:

$$V_{ij} = \frac{q_i q_j}{r} + A_{ij} e^{-B_{ij} r}.$$

For the charge $q(\mathrm{O})$ of the oxygen centers as well as for the charge $q(\mathrm{Li})$ of the lithium centers in Li_4O and for the parameters A and B we used the values of reference [22] and in order to reproduce various experimental data for the $q(\mathrm{Li})$ charge of the Li centers in Li_nO_m, we used $q(\mathrm{Li}) = \frac{mq(\mathrm{O})}{m}$. For species with a large number of Li atoms, the pair-wise potential V_{ij} is no longer adequate

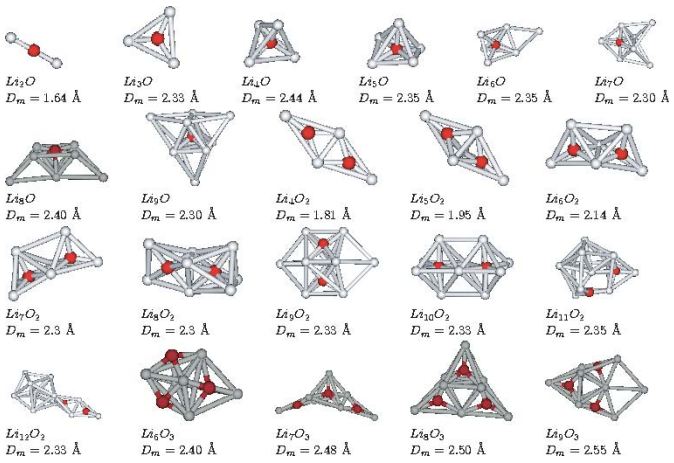

Fig. 3. Ab initio structure of Li_nO_m clusters obtained with Gaussian 98.

to represent, even roughly, cluster energies. For these cases, energies have been calculated using a semi-empirical method namely AM1 [23]. For a lot of randomly chosen geometries, energy minimization is performed through gradient techniques and from these numerous results stable isomers are selected. We present in Figure 3 the geometry of the most stable isomer for the Li_nO_m clusters of interest.

In order to obtain adiabatic ionization potentials, stable structures for the corresponding cations $Li_nO^+_{1,2,3}$ are obtained through a gradient process using as initial geometries that ones previously determined for the corresponding neutral species, energies being calculated with the DFT/PW91 method. Ionization potentials are then calculated as $E(Li_nO_m) - E(Li_nO^+_m)$. Vertical *IP* corresponds to the cation energy evaluated for the geometry of the neutral while for the adiabatic *IP* the geometry of the cation is optimized.

The optimized cation structures are not displayed in Figure 3 because they were seen to be very similar to that obtained for the neutral clusters. As a sign of their differences we have determined for both the neutral and its cation structures an average bond length $\overline{r} \cdot \overline{r}$ defined as follows:

$$\overline{r} = \sum_{i=1}^{6+p} \frac{\overline{D}_i}{6+p}$$

where

$$\overline{D}_i = \sum_{j=1}^{N} \frac{d_{ij}}{N}$$

d_{ij} is the distance between the atom i and one of its N nearest neighbors. Differences between the values of $\overline{r}$ for the neutral and its cation were found to be less than 2%. The calculated vertical and adiabatic ionization potentials are summarized in Table 2, and compared to the experimental values. The agreement is roughly good, with no differences above 0.5 eV.

Table 2. Calculated values for vertical and adiabatic ionization potentials in eV. The values are compared to the experimental values.

Compound	IP_{vert}	$IP_{vert} - IP_{exp}$	IP_a	$IP_a - IP_{exp}$
Li_2O	6.53	()	6.25	()
Li_3O	4.36	(+0.8)	3.85	(+0.3)
Li_4O	4.26	(+0.1)	4.25	(+0.09)
Li_5O	4.25	(+0.25)	4.04	(–0.01)
Li_6O	4.27	(–0.43)	4.12	(–0.58)
Li_7O	4.29	(+0.24)	4.15	(+0.10)
Li_8O	4.32	(+0.07)	3.67	(–0.58)
Li_9O	4.47	(+0.60)	4.36	(0.49)
$Li_{10}O$	4.29	(+0.24)	4.25	(0.20)
Li_4O_2	5.49	(+0.53)	5.33	(+0.37)
Li_5O_2	3.35	(+0.71)	3.36	(+0.72)
Li_6O_2	3.59	(–0.06)	3.57	(–0.08)
Li_7O_2	3.80	(+0.36)	3.60	(+0.16)
Li_8O_2	4.06	(+0.09)	3.98	(+0.03)
Li_9O_2	3.80	(+0.32)	3.72	(+0.24)
$Li_{10}O_2$	4.12	(+0.32)	4.00	(+0.20)
$Li_{11}O_2$	4.01	(+0.53)	3.78	(+0.30)
$Li_{12}O_2$	4.32	(+0.51)	4.04	(+0.23)
Li_6O_3	4.60	(–0.36)		
Li_7O_3	3.47	(+0.91)		
Li_8O_3	3.41	(–0.03)		
Li_9O_3	3.91	(+0.47)		

4 Analyze and discussion

Metal-rich clusters

As oxygen is a divalent element, one oxygen atom is attempted to localize the valence electrons from only two lithium atoms, leaving the remaining valence electrons delocalized within the cluster. Indeed, evidence of this phenomenon has been seen on Li_nO clusters by Lievens et al. [12]. The ionization potentials of Li_nO clusters present odd-even alternation and energy gaps for $n = 10, 22$, and 42, as it appears in pure lithium clusters, but for sizes shifted by two: $n = 8, 20$, and 40. This is in agreement with the spherical shell model of metallic clusters. As a consequence, monoxide lithium clusters can be seen as constituted by an ionic part (Li_2O) and a metallic one Li_p, with $p = n-2$. To search for similar or contradictory signs, the ionization potentials of Li_nO_m ($m = 1, 2, 3$) clusters are shown in Figure 4 versus the number $p = n - 2m$ of supposed delocalized electrons. The first striking feature is the general similarity of these three curves. One of the sign of a metallic behavior appears, with an odd-even alternation of the *IP* values. Furthermore, those *IP* values of large size clusters tend towards a 3.5 eV limit, close to this of bare lithium clusters (3.3 eV). It has already been noticed by Lievens et al. that increasing the Li_nO cluster size the influence of the oxygen atom becomes negligible in the *IP* values. Indeed, it is reasonable to think that the role of one and even three oxygen atoms is similar and

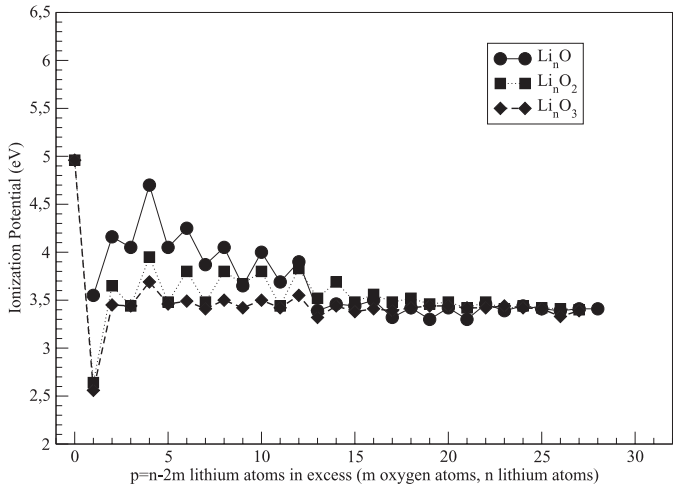

Fig. 4. Ionization potentials of metal-rich $Li_p(Li_2O)_m$ clusters.

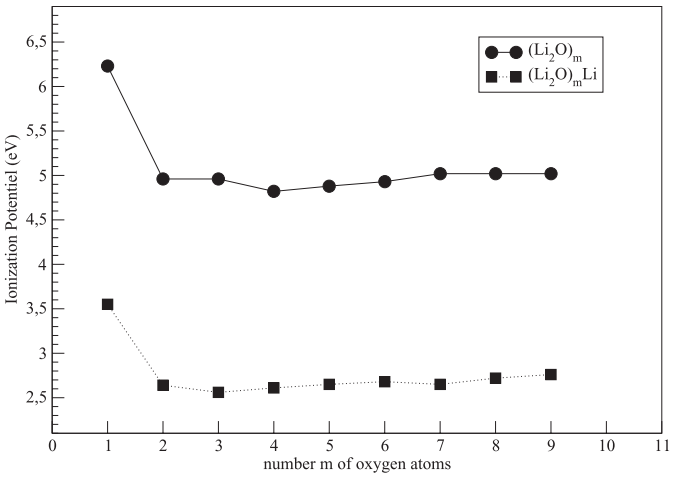

Fig. 5. Ionization potentials of stoechiometric and sub-stoechiometric cluster.

that the clusters develop rapidly the metallic characteristics of bare Li_n for increasing n values. Of great interest is the comparison of this result with the calculated geometries found for Li_nO_m clusters; they show that in most of the case the oxygen atoms are embedded inside the cluster, surrounded by at least three lithium atoms. So, if according to *IP* values, a metallic behavior characterized by valence electrons delocalization seems to be present, it is not clear that this effect corresponds to a geometrical segregation between two ionic and metallic clusters like in Li_nH_m clusters, where the structure is an association of two $(LiH)_m$ and Li_p clusters. The lithium-oxide clusters structures are closer to those of barium-oxide, pointing out a coherent behavior of oxygen on which we will come later. Furthermore, we should notice that no clear energy gaps are seen in our results at the close shell sizes $p = 8$ and 20. Similarly the odd-even alternation is less and less pronounced with an increasing number of oxygen atoms.

Near stoechiometry clusters

It is striking to see that the *IP* evolution of stoechiometric $(Li_2O)_m$ clusters is very similar to what we already observed on $(BaO)_m$ clusters [5]. A large gap (1.3 eV) is observed between the Li_2O molecule *IP* and the first cluster $(Li_2O)_2$ (see Fig. 5). The Li_2O bulk is an isolator crystal with a band gap of 4.6 eV and a work function estimated less than one eV below this value. So it appears that the *IP* of the $(Li_2O)_m$ clusters are all close to the bulk work function, even for the smallest one $(Li_2O)_2$. Referring to ab initio AIMD calculations performed by Finocchi et al. [24] on $(Li_2O)_m$ clusters, for $m = 2$ to 6 and our Gaussian calculations (see Tab. 2), limited to $m = 4$, it appears that the D_{mean} values increases with m and that the bulk value is reached beyond $m = 6$. Nevertheless according to our experimental results, and regarding the *IP* values, the bulk properties are observed all along the $(Li_2O)_m$ cluster series and they start at the very beginning of the series for $n = 2$. The equilibrium geometries determined by these above calculations exhibit a high compacity for the smaller clusters, therefore all those structures are completely governed by electrostatic interactions Li and O atom.

In opposite to these high *IP* values, those of clusters containing one excess lithium atom $(Li_2O)_mLi$ appear very low, with values close to 2.5 eV. In our calculations it appears for those clusters a free electronic density region. This situation is similar to the "F-center" type structure of the Ba_nO_{n-1} as well as the additional free electronic density created in a stoechiometric Na_nF_n cluster by the addition of an external Na atom. This excess electronic density is responsible for the drastic decrease in the *IP* value when adding one metallic, electropositive atom to a pure ionic cluster.

From metal-rich to stoechiometric clusters: transition in the influence of oxygen atoms

From the two previous paragraphs, it appears that the rate of oxygen is fundamental in determining the clusters behavior. We then propose to plot the *IP* values versus the ratio m/n of oxygen in a Li_nO_m cluster. By doing so, the specific behavior of oxygen in metallic clusters appears (see Fig. 6). Three parts can be distinguished:

- when the ratio of oxygen is roughly below 0.35, the ionization potentials values are stable between 3.3 and 4.0 eV;
- for an oxygen ratio above 0.35, the ionization potential decreases to reach the smallest values of the $(Li_2O)_mLi$ clusters;
- finally, between $(Li_2O)_mLi$ and $(Li_2O)_m$ clusters, a large gap of roughly 2.5 eV is observed.

Before proceeding to the analyze of this particular behavior, we should notice that these results are in agreement with those of Bréchignac and coworkers obtained with an evaporation experiment on Li_nO_m clusters [25]. It is striking that by another way, they also conclude to the loss

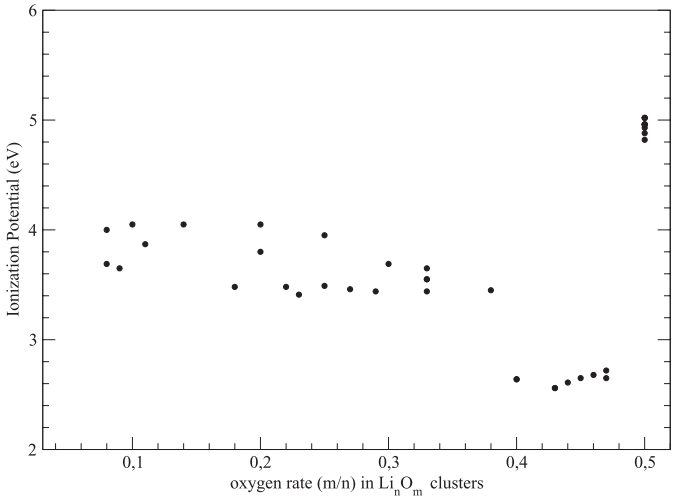

Fig. 6. Ionization potentials of Li_nO_m clusters versus the rate m/n of oxygen.

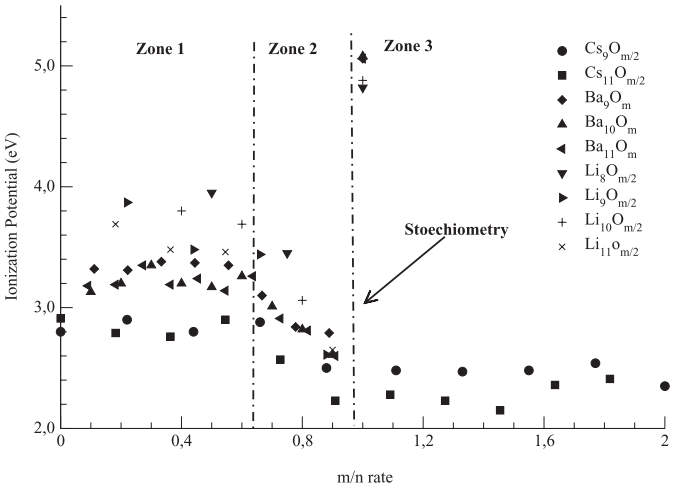

Fig. 7. Ionization potentials of Cs_nO_m, Ba_nO_m compared with Li_nO_m clusters versus the ratio m/n of oxygen.

of metallicity in $(Li_2O)_mLi_p$ clusters for which the ratio $x = p/(p+2m)$ is below 0.4. Yet this ratio is linked to the ratio of oxygen atoms in the cluster : $m/n = (1-x)/2$. So $x \leq 0.4$ is equivalent to $m/n \leq 0.3$, which is a value very close to the 0.35 we found. The first and the third parts of this curve have already been explained in the two previous paragraphs.

Below 35% of oxygen, the clusters are metal-rich ones, in which the oxygen atoms do not influence the ionization potential. Indeed electron is extracted from the metallic region rather than from area where oxygen is present. For this reason the metallic part of the cluster governs the *IP* value in the same way as in pure metallic clusters as long as the oxydated region is small as compared to the metallic one. For increasing m/n values a new effect occurs, the electronic energy levels of the metallic part are modified as explained by Martin and coworkers in their study of cesium oxides clusters [10]. With the assumption that the oxygen atoms bind up to two electrons from the cesium atoms, the so-formed negative oxygen ion acts as a barrier repelling the conduction electrons. The free electrons are then constrained to move in a smaller volume as compared to pure metal clusters; as m/n values increase, the electronic volume decreasing becomes more and more significant. In the electronic shell model, this leads to a decrease of the ionization potential. Our geometrical calculations, as well as those of Finocchi and coworkers, show that valence electrons brought by lithium atoms to a stoechiometric $(Li_2O)_m$ cluster are involved in $Li-O$ bonds. The mean value of the interatomic distances inside the cluster reaches a constant around 2.35 ± 0.1 Å in $Li_{4+p}O_2$ clusters (resp. $Li_{6+p}O_3$), for $Li-Li$ bonds for $p \geq 3$ (resp. $p \geq 2$) (Fig. 3). The value $p \geq 3$ found by Finocchi et al. for $Li_{4+p}O_2$ clusters, indicates also that substoechiometric $(Li_2O)_mLi_p$ clusters do not necessarily contain metallic Li atoms. For these clusters, in which all the electrons are involved in bonds with the O atoms, they have computed a HOMO at the highest energy, thus leading to a small ionization potential. In this scenario, the decrease in Li_nO_m *IP* for an oxygen ratio above 35% reveals an electronic change in the clusters. It marks the end of a segregated cluster containing metallic Li atoms. The behavior of Cs_nO_m clusters appears to be very similar to Li_nO_m clusters ones. Plotting TP Martin results in the same way as ours leads to Figure 6. The decrease of the *IP* curve for an oxygen ratio greater than 40% also appears. Furthermore, the small *IP* values found for stoechiometric $(Cs_2O)_m$ clusters can be attributed to a similarity with the semi-conductor Cs_2O bulk structure. At this point, it is interesting to compare this result with what we previously found for barium oxide clusters. Indeed, the same general evolution of the *IP* versus the oxygen ratio in the clusters is observed. The decrease begin at 60% in Ba_nO_m, which is comparable with the 35% in Li_nO_m, by tacking into account the different stoechiometry (one Ba atom for one O atom, and 2 Li atoms for one O atom). However, abinitio calculations on the smallest Ba_nO_m clusters, completed by a simple electrostatic model, led us to give an explanation based on the cluster geometry [18]. The icosahedral close-packing structure of pure barium clusters allows the insertion of a small number of O atoms with conservation of this particular structure. The 60% of oxygen ratio after which the *IP* curve decreases corresponds to a breakdown of the bare barium clusters skeleton, when there is no more place for O atoms. This scenario can not be adopted for lithium oxide clusters, which structure is found completely different from bare clusters by calculations. Indeed the small size lithium clusters jellium do not drive a specific geometry. The oxygen atom presents this particular behavior to be surrounded by all the lithium atoms, regarding the growth of Li_nO_m clusters families no elementary minimum geometry structure appears as it is shown in Figure 3.

Furthermore, the similarity of the critical ratio, when taking into account the different stoechiometry, supports an electronic factor.

5 Conclusion

Those results on Li_nO_m clusters are quite similar to former measurements of ionization potentials of alkaline earth suboxide Ba_nO_m and alkaline suboxide Cs_nO_m clusters. So we can confirm the initial idea that oxygen atom plays a specific role when associated to metal atoms inside the cluster as compared with the electronegative elements: halogens or hydrogen where the ionic character of the bonding with the metal atom has been demonstrated and leads to a clear segregation into two adjacent parts of halides or hydrides in one hand and metallic cluster on the other hand. On the contrary the oxygen atom establishes iono-covalent bonding with several surrounding metal atoms; it is completely embedded inside the structure. Moreover this process leads to a contraction characterized by a decreasing about 25% of the mean interatomic distance value, which is not observed in any other elctronegative-metal clusters. This specific behavior is responsible for the appearance of a zone 2 in ionization potentials in Figure 6.

References

1. R. Antoine et al., J. Chem. Phys. **104**, 110 (1996)
2. P.J. Ziemann, A.W. Castelman Jr, J. Chem. Phys. **94**, 718 (1991)
3. D. van Heijnsbergen, G. von Helden, G. Meijer, M.A. Duncan, J. Chem. Phys. **116**, 2400 (2002)
4. T.P. Martin, T. Bergmann, J. Chem. Phys. **90**, 6664 (1989)
5. V. Boutou, M.A. Lebeault, A.R. Allouche, F. Paulig, J. Viallon, C. Bordas, J. Chevaleyre, J. Chem. Phys. **112**, 6228 (2000)
6. M. Foltin, G.J. Stueber, E.R. Bernstein, J. Chem. Phys. **114**, 8971 (2001)
7. B. Vezin, P. Dugourd D. Rayane, P. Labastie, J. Chevaleyre, M. Broyer, Chem. Phys. Lett. **206**, 521 (1993)
8. P. Labastie, J.M. L'Hermite, Ph. Poncharal, M. Sence, J. Chem. Phys. **103**, 6362 (1995)
9. V. Boutou, A.R. Allouche, F. Spiegelmann, J. Chevaleyre, M.A. Frecon, Eur. Phys. J. D **2**, 63 (1998)
10. H.G. Limberger, T.P. Martin, J. Chem. Phys. **90**, 2979 (1989)
11. P. Dugourd, D. Rayane, P. Labastie, B. Vezin, J. Chevaleyre, M. Broyer, Chem. Phys. Lett. **197**, 433 (1992)
12. P. Lievens, P. Thoen, S. Bouckaert, W. Bouwen, F. Vanhoutte, H. Weidele, R.E. Silverans, Chem. Phys. Lett. **302**, 571 (1999)
13. V. Boutou, M.A. Lebeault-Dorget, A.R. Allouche, C. Bordas, J. Chevaleyre, Z. Phys. D **40**, 448 (1997)
14. W.A. de Heer, Rev. Mod. Phys. **65**, 611 (1993)
15. M.M. Kappes, M. Schär, U. Röthlisberger, C. Yeretzian, E. Schumacher, Chem. Phys. Lett. **143**, 251 (1988)
16. E.C. Honea, M.L. Homer, J.L. Persson, R.L. Whetten, Chem. Phys. Lett. **171**, 147 (1990)
17. P. Lievens, P. Thoen, S. Bouckaert, W. Bouwen, E. Vandeweert, F. Vanhoutte, H. Weidele, R.E. Silverans, Z. Phys. D **42**, 231 (1997)
18. V. Boutou, M.A. Lebeault, A.R. Allouche, C. Bordas, F. Paulig, J. Viallon, J. Chevaleyre, Phys. Rev. Lett. **80**, 2817 (1998)
19. M.J. Frish, G.W. Trucks, H.B. Schlegel, et al., *Gaussian 98*, Gaussian Inc., Pittsburgh, PA, revision a7 edition, 1998
20. J.P. Perdrew, K. Burke, Y Wang, Phys. Rev. Lett. **54**, 16533 (1996)
21. A.D. Becke, J. Chem. Phys. **104**, 1040 (1996)
22. F. Finocchi, C. Noguera, Phys. Rev. B **57**, 14646 (1998)
23. M.J.S. Dewar, E.G. Zoebisch, E.F. Healy, J.P. Stewart, J. Am. Chem. Soc. **107**, 3902 (1985)
24. F. Finocchi, C. Noguera, Phys. Rev. B **53**, 4989 (1996)
25. C. Brechignac, P. Cahuzac, M. de Frutos, P. Garnier, Z. Phys. D **42**, 303 (1997)